

# Analysing QBER and secure keyrate under various losses for satellite based free space QKD

Muskan\*, Ramniwas Meena†, Subhashish Banerjee‡

Department of Physics, Indian Institute of Technology, Jodhpur, India-342030

January 2024

## Abstract

Quantum key distribution (QKD) is a method that uses the qubits to safely distribute one-time use encryption keys between two or more authorised participants in a way that ensures the identification of any eavesdropper. This work delves into the atmospheric transmittance relationship with zenith angle during uplink night-time and day-time/night-time downlink scenarios. We have also done a comparison between the QBER and keyrate performance of the BB84 and B92 protocols, as well as the BBM92 and E91 entangled-based protocols for laser links between a ground station and a satellite in low Earth orbit. The change in comparative efficiency between these protocols based on varying zenith angles show-cases the dynamic nature of their performance characteristics, highlighting how their advantages and disadvantages manifest under different operational conditions.

**Keywords**— Quantum cryptography, Quantum communication, Free space communication

## 1 Introduction

The most developed use of quantum communication is quantum cryptography [1–5] which offers a completely secure coding mechanism. In order to provide secure quantum optical communication, quantum key distribution (QKD) uses the qubits to safely distribute one-time use encryption keys between two or more authorised participants in a way that ensures the identification of any eavesdropper. Heisenberg’s uncertainty principle and the quantum no-cloning principle provide assurance for QKD security [6, 7]. Essentially, a solution to the key distribution problem is devised by leveraging these physical characteristics of the information carrier to prevent eavesdropping. Any information obtained by an illegitimate third party about the exchanged key leads to a corresponding increase in the quantum bit error rate (QBER) of the transmitted data.

The concept of QKD was initially proposed in [8]. In [9], the first implementation of free space QKD over a 30 cm optical link was demonstrated. Since then, significant research efforts have been dedicated to developing this technology for future optical communication systems that support secure transmission of critical information. While early experimental setups were capable of sending quantum signals over distances of up to 100 km [10] using optical fiber links, the propagation limitations of optical fibers restricted QKD over fibers to only a few hundred kilometers [11]. However, using free space links offers the potential to extend these distances further [12, 13]. Free space links leverage low absorption in specific wavelength ranges and non-birefringent characteristics, ensuring the preservation of polarization. To fully harness the advantages

---

\*E-mail: muskan.1@iitj.ac.in

†E-mail: meena.53@iitj.ac.in

‡E-mail: subhashish@iitj.ac.in

of free space communication, satellites are ideal [14]. By utilizing satellites in Earth satellite links, the path within the atmosphere can be reduced to approximately 30 km (depending on satellite elevation). Establishing a network of satellites would enable a physically secure global communication network, thereby significantly expanding the range of QKD capabilities.

In the construction of a worldwide network, satellite-based quantum communication is crucial and effective [15–23]. Free space QKD under atmospheric turbulence must be taken into account for the successful implementation of satellite-based quantum communication [24–27]. For earth-to-space quantum communication to be possible, the connection attenuation must be less than 60 dB; quantum communication is not practical above this number. The following situations between Earth and space have the following link distances (L): Ground-low earth orbit (LEO) and LEO-ground link distances are 500-1400 km, Ground-medium earth orbit (MEO) and MEO-ground link distances are 5000-20000 km, ground-geostationary earth orbit (GEO) and GEO-ground link distances are above 36,000 km. Quantum communication still requires additional research to address problems with security, data rate, and communication distance despite the huge success of QKD’s commercial applications in terms of scientific advancement [28–32].

The process of generating a secret key using QKD involves five essential steps: authentication [33, 34], single photon transmissions, sifting, error correction, and privacy amplification [35]. Initially, a randomly generated raw key is transmitted over the quantum channel to create secret key information. Following this, the key information is exchanged over a public channel, resulting in the acquisition of the sifted key. Subsequently, error correction and privacy amplification steps are employed. The purpose of the error correction step is twofold: it corrects any errors in the received information bits and provides an estimation of the error rate. On the other hand, privacy amplification is implemented to distill a shorter yet significantly more secure final key as desired.

When assessing the effectiveness of different QKD systems, two important criteria are considered: the *QBER* and the *keyrate*. The *QBER* serves as an indicator of security and is crucial for evaluating the performance of the link after error correction. If an unauthorized third party gains any knowledge about the exchanged key, it leads to an increase in the *QBER*. A higher *QBER* means that the eavesdropper can gather more information about the transmitted key, compromising the security of the legitimate recipient. We have studied how the atmospheric transmittance is linked to the zenith angle in both night-time uplink (ground-to-satellite) and day/night downlink (satellite-to-ground) situations. We have also done theoretical study analyzing well-known QKD protocols BB84 and B92, alongwith entangled-based protocols BBM92 and E91, specifically examining their performance in both uplink and downlink scenarios. Our focus will be on understanding how the characteristics of the free-space channel, including factors like scattering and turbulence, affect crucial parameters such as *QBER* and *keyrate*. Additionally, we aim to compare these protocols based on their performance regarding *QBER* and *keyrate* metrics.

The paper is structured as follows: Sec. 2 provides a concise analysis of the BB84, B92, BBM92, and E91 protocols. Sec. 3, covers channel modeling, encompassing different types of loss factors such as geometrical, scattering, and turbulence. Sec. 4 then delves into environmental noise, specifically addressing stray counts. Next, in Sec. 5, we introduce and analyze the *QBER* for different protocols. Sec. 6 focuses on the *keyrate* calculations for different protocols. In Sec. 7, we present numerical results and have discussions. The paper concludes with a summary of the key points.

## 2 QKD Protocols

QKD protocols are the foundation of secure communication enabled by quantum mechanics. These protocols establish a shared secret key between two parties, typically referred to as Alice and Bob, while ensuring that any eavesdropping attempts are detectable. Several QKD protocols have been developed, each with its unique approach to key generation and security guarantees. Here we briefly discuss the QKD protocols used in this work:

## 2.1 BB84

The BB84 protocol, which was proposed in [8], is a QKD protocol. It aims to facilitate the secure generation and sharing of a secret cryptographic key between two parties, typically referred to as Alice and Bob, for subsequent communication purposes. In this protocol, Alice prepares a random string of qubits, which can be in the states  $|0\rangle$ ,  $|1\rangle$ ,  $|+\rangle$ , or  $|-\rangle$ , and transmits them to Bob. Upon receiving the qubits, Bob randomly measures each qubit in either the standard basis  $0, 1$  or in the Hadamard basis  $+, -$  and publicly announces the basis used for each measurement. Alice then informs Bob about the cases where Bob's basis matches her own. Only the qubits measured using the same basis by both Alice and Bob are retained, while the rest are discarded. It is expected that, on average, Bob's basis will match Alice's basis 50% of the time. In an ideal scenario, the retained qubit strings of Alice and Bob are perfectly symmetric. To verify the correctness of the generated key, Bob uses a portion of the string as a verification string and publicly announces the measurement results and corresponding positions of these qubits. Alice compares Bob's results with her own. If the number of errors exceeds a tolerable limit, the protocol is discarded. Otherwise, a perfectly symmetric, random, and unconditionally secure quantum key is obtained.

## 2.2 B92

The B92 protocol, a simplified version of the BB84 protocol, is another QKD protocol [36]. Unlike BB84, the B92 protocol only uses two quantum states,  $|0\rangle$  and  $|+\rangle$ , for transmitting information. In this protocol, Alice randomly sends a string of  $|0\rangle$  and  $|+\rangle$  to Bob, where  $|0\rangle$  corresponds to bit value 0 and  $|+\rangle$  corresponds to bit value 1. The main difference between BB84 and B92 lies in the number of states used for transmission. While BB84 uses four states ( $|0\rangle$ ,  $|1\rangle$ ,  $|+\rangle$ ,  $|-\rangle$ ), B92 uses only two ( $|0\rangle$ ,  $|+\rangle$ ). Bob measures the incoming qubits randomly in one of the two bases:  $|0\rangle$ ,  $|1\rangle$  or  $|+\rangle$ ,  $|-\rangle$ . However, in the B92 protocol, Bob does not announce the basis he used for measurement. He keeps the qubits where his measurement outcome is  $|1\rangle$  or  $|-\rangle$ , discarding all other qubits. Bob then announces which qubits are to be kept. Following Bob's announcement, Alice also keeps the corresponding qubits (partner qubits) and discards the rest. If Bob's measurement yields  $|0\rangle$ , he cannot determine whether Alice has sent  $|0\rangle$  or  $|+\rangle$ , as the  $|+\rangle$  state measured in the computational basis will collapse to  $|0\rangle$  50% of the time. Consequently, if Bob's measurement yields  $|0\rangle$ , he cannot infer the encoding used by Alice. Furthermore, if Alice sends  $|0\rangle$ , Bob will never receive it as  $|1\rangle$ . This is because if Bob chooses the computational basis, he will always measure it as  $|0\rangle$ , and if he chooses the diagonal basis, he will obtain  $|+\rangle$  or  $|-\rangle$  with equal probability. Thus, Bob's measurement can only yield  $|1\rangle$  if Alice has sent  $|+\rangle$ . Therefore, whenever Bob's measurement yields  $|-\rangle$ , he can conclude that Alice has sent him  $|0\rangle$ . However, he cannot draw any conclusions when his measurement yields  $|+\rangle$ . Since Bob knows the encoding, the remaining string can be used to generate a random symmetric key.

## 2.3 E91

The E91 QKD protocol, introduced in [37], relies on entanglement. Here's a simplified overview of the procedure: A source distributes maximally entangled qubit pairs, such as the state  $|\psi^-\rangle_{AB} = \frac{1}{\sqrt{2}}(|01\rangle_{AB} - |10\rangle_{AB})$ , to Alice and Bob. Alice and Bob randomly select observables  $\{A_i\}$  and  $\{B_i\}$  and measure the qubit pairs using spin components in the Bloch sphere's  $x-z$  plane as shown in Fig.1. Measurement operators are defined as  $A_i = \cos \varphi_i^A + \sin \varphi_i^A$  and  $B_i = \cos \varphi_i^B + \sin \varphi_i^B$ , with specific angles for Alice and Bob. Measurement directions, represented by  $Z$  and  $X$ , can also be expressed as  $A_1 = B_1 = Z$ ,  $A_2 = X$ ,  $B_2 = \frac{1}{\sqrt{2}}(Z - X)$ ,  $A_3 = \frac{1}{\sqrt{2}}(Z + X)$ , and  $B_3 = \frac{1}{\sqrt{2}}(Z + X)$ . Measurement outcomes, like  $(A_1, B_1)$  and  $(A_3, B_3)$ , with matching directions, yield totally anti-correlated outputs, constituting the sifted key. To assess eavesdropper knowledge, measurement pairs  $(A_1, B_3)$ ,  $(A_1, B_2)$ ,  $(A_2, B_3)$ , and  $(A_2, B_2)$  are analyzed using a CHSH inequality. The CHSH inequality violation ( $S = 2\sqrt{2}$ ) confirms maximal entanglement between Alice and Bob, ensuring Eve's lack of knowledge about the key. Privacy amplification and error correction can be applied to obtain the final secret key if the measurement findings pass the test.

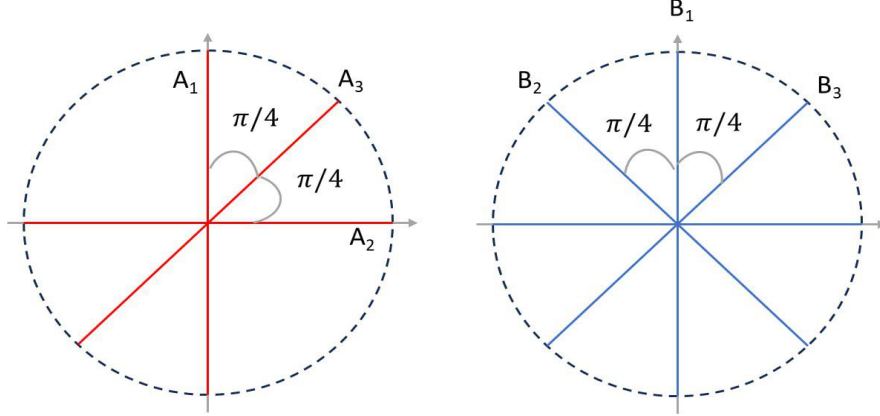


Figure 1: Measurements directions for the Ekert protocol. The measurements are depicted in the  $x$ - $z$  plane of the Bloch sphere. On the left side are the three different measurements that Alice can choose between, and on the right side Bob's possible measurement directions are shown.

## 2.4 BBM92

BBM92 is another entangled based protocol. The protocol was first proposed in 1992 [38]. The protocol makes use of pairs of entangled particles, known as EPR pairs, which are distributed between Alice and Bob. Here's how the BBM92 protocol works: Alice creates a set of EPR pairs and sends one particle from each pair to Bob. Bob randomly measures each incoming particle using one of two bases: the standard basis (Z-basis) or the Hadamard basis (X-basis). Alice tells Bob which basis she used to prepare each particle. Bob discards all the measurements that were made in the wrong basis, and keeps the rest. Alice and Bob publicly compare a subset of their remaining measurements to estimate the error rate. Alice and Bob use the remaining measurements to generate a secret key by applying a reconciliation procedure and a privacy amplification procedure. Alice and Bob can now use their secret key for secure communication. The BBM92 protocol is secure against eavesdropping because any attempt to measure the particles in transit will disturb the entanglement and be detected by Alice and Bob. Additionally, the use of entangled pairs ensures that any attempt to clone the particles will also be detected.

## 3 Channel Modeling

Channel modeling for satellite communication is a critical aspect of designing and optimizing satellite communication systems. It involves the study and characterization of the transmission medium between the satellite and ground station. For the communication with Gaussian light beam the channel transmittance can be affected by various losses of environment parameters, i.e., scattering particles or molecules, turbulence medium. Here, we assume that all losses are uncorrelated. Thus, the overall transmittance efficiency ( $\eta_T$ ) considering multiple loss factors can be determined by

$$\eta_T = \eta_{geo} * \eta_t * \eta_r * \eta_{scatt} * \eta_{turb} * \eta_{bw}. \quad (1)$$

Here  $\eta_t$  and  $\eta_r$  represent the efficiency of the transmitter and receiver, respectively and  $\eta_{geo}$ ,  $\eta_{scatt}$ ,  $\eta_{turb}$  and  $\eta_{bw}$  represent the transmittance factor due to geometrical, scattering, turbulence and beam-wandering. Other parameters related to losses are described in detail in the following subsection.

### 3.1 Geometrical Factor

Geometrical factor is a measure of the reduction in signal power as it propagates from a transmitter to a receiver. It is determined by the ratio of the surface area of the receiver aperture to the surface area of the transmitter beam at the receiver [39, 40]. The surface area of the transmitter beam is affected by its divergence, which causes it to spread out as it travels through space. Therefore, geometrical factor is primarily influenced by the divergence of the beam and the distance between the transmitter and receiver. The geometrical factor can be determined by the formula stated as:

$$\eta_{geo} = \frac{d_r^2}{(d_t + (L\theta))^2}. \quad (2)$$

Here,  $d_r$  represents diameter of the receiver (in m),  $d_t$  represents diameter of the transmitter (in m),  $\theta$  is divergence angle of the beam (in mrad), L is the distance between transmitter and receiver.

### 3.2 Scattering

The primary factors contributing to loss in the atmospheric channel are absorption and scattering processes [41]. Absorption in the atmosphere occurs when the photons of the beam interact with dispersed particles such as water vapors, dust, ice, and organic molecules. However, it's important to note that atmospheric absorption is dependent on the wavelength of the beam. To minimize absorption effects, the wavelength range of FSO (Free-Space Optical) communication systems is carefully selected to ensure minimal absorption.

Scattering refers to the phenomenon where a beam of radiation is dispersed into various directions due to physical interactions. Rayleigh scattering occurs when molecules and atmospheric gases scatter light with sizes significantly smaller than the wavelength of the incident light. Mie scattering occurs when the diameter of particles is equal to or larger than one-tenth of the wavelength of the incident laser beam. In the context of FSO at terrestrial altitudes, Mie scattering is the primary cause of attenuation at the laser wavelengths used. Fog and haze droplets, which dominate the Mie-scattering effect, are responsible for the significant attenuation of transmitted optical beams in free space. Non-selective scattering refers to the scattering phenomenon caused by rainfall, where the radius of raindrops is considerably larger than the wavelength of typical FSO systems. Due to this size difference, the laser beam is capable of passing through raindrops or particles with minimal scattering effects. Hence attenuation is mainly due to Mie-scattering.

The measurement of atmospheric visibility provides a valuable indication of the prevailing environmental conditions in the atmosphere. Visibility is the distance that a parallel luminous beam can travel through the atmosphere until its intensity decreases by 2% of its original value. This measurement is conducted using a wavelength of 550nm, which corresponds to the wavelength that the human eye is most sensitive to.

Mie scattering theory can be utilized to predict the attenuation caused by fog. The specific attenuation of fog given by common empirical model for Mie scattering [42] can be written as follow at altitude h -

$$\beta(\lambda, h) = \frac{3.91}{V(h)} \left( \frac{\lambda}{550} \right)^{-P(h)}, \quad (3)$$

where  $V(h) = 3V_0h^{0.26}$  stands for visibility range ( $V_0$  is visibility at  $h_0$  altitude) [43],  $\lambda$  is the operating wavelength and  $P(h)$  is the size distribution coefficient of scattering. According to Kruse Model [42]

$$P(h) = \left\{ \begin{array}{ll} 1.6 & V(h) > 50km \\ 1.3 & 6km < V(h) < 50km \\ 0.585V(h)^{1/3} & V(h) < 6km \end{array} \right\}. \quad (4)$$

The transmittance factor due to the scattering can be written as follow

$$\eta_{scatt} = \exp\left(-\int_{h_t}^{h_r} \beta(\lambda, h) dh\right), \quad (5)$$

where  $h_t$  and  $h_r$  are altitude height of transmitter and receiver respectively.

### 3.3 Turbulence-Induced Scintillation Loss

In the realm of satellite-ground communication for both uplink and downlink, the optical signals traverse the earth's atmosphere and experience power loss attributed to diverse factors such as geographical surroundings, time of day, and weather conditions. Furthermore, the daytime presents higher levels of atmospheric turbulence compared to the night [44]. The duty of an FSO system designer is to meticulously assess design requirements with the aim of minimizing signal attenuation caused by atmospheric conditions. This work delves into the atmospheric attenuation factors impacting both satellite-to-ground and ground-to-satellite communications. When it comes to the uplink, turbulence becomes a factor only in the initial segment of the path. Beyond the upper atmospheric layers, turbulence doesn't impede the signal propagation. The turbulence effect is more pronounced in the uplink because the beam encounters distortion early in its atmospheric journey before entering free space. Conversely, in the downlink, the laser beam traverses the first 99% of the total distance without encountering interruptions, making the impact of scintillation less severe compared to the uplink scenario. Details can be seen in Appendix A.

Scintillation loss of the transmission system (in dB) is given by [45]:

$$a_{sci} = [3.3 - 5.77(-\ln p_{thr})^{\frac{1}{2}}](\sigma_I^2(d_r))^{0.4}. \quad (6)$$

Here  $p_{thr}$  is the probability that the receiver power falls below the minimum received power. In our analysis, the scintillation loss is expressed as a function of height and is implicitly included in  $\sigma_I^2(d_r)$  which is the magnitude of scintillation described in the Appendix A.

The transmittance factor due to the turbulence can be written as follows

$$\eta_{turb} = 10^{a_{sci}/10}, \quad a_{sci} < 0. \quad (7)$$

### 3.4 Turbulence-Induced Beam Wandering Effect

In the satellite-ground FSO link, as the laser beam traverses the atmosphere, it undergoes distortions. These distortions extend beyond the typical diffraction-induced spreading, encompassing random shifts in the beam's centroid (beam wander) and unpredictable redistributions of energy within the beam's cross-section (irradiance fluctuations). These effects are manifestations of wavefront distortions induced by atmospheric turbulence [46].

When the turbulence eddies surpass the size of the laser beam, a phenomenon known as beam wander occurs. In this scenario, the beam experiences random deflections from its intended propagation path, leading to potential link failures. On the uplink, the laser beam undergoes distortion near the transmitter due to atmospheric turbulence. Consequently, as the laser beam propagates over an extended distance, it contends with free space diffraction effects. The scintillation produced by beam wander effect is expressed as [47]:

$$\sigma_{I,l}^2(L) = 5.95(H - h_0)^2 \sec^2(\theta) \left(\frac{2W_0}{r_0}\right)^{5/3} \left(\frac{\alpha_{Pe}}{W}\right)^2. \quad (8)$$

In the above equation,  $\alpha_{Pe} = \sigma_{Pe}/L$  is the angular pointing error due to beam wander effect and  $\sigma_{Pe}$  and other parameters are described in Appendix B.

Beam wandering loss of the transmission system (in dB) is given by [45]:

$$a_{bw} = [3.3 - 5.77(-\ln p_{thr})^{\frac{1}{2}}](\sigma_{I,l}^2(L))^{0.4}. \quad (9)$$

Here  $p_{thr}$  is the probability that the receiver power falls below the minimum received power. The transmittance factor due to the Beam wandering can be written as follows

$$\eta_{bw} = 10^{a_{bw}/10}, \quad a_{bw} < 0. \quad (10)$$

## 4 Environmental Photons (stray-photons)

In free-space communication, environmental photons represent a significant noise source. Here, we'll summarize the analysis concerning the impact of these environmental photons on the detector, both for downlinks and uplinks, which is crucial in calculating the QBER. For uplinks, we only consider the case of night-time operation. If the ground station site has a low level of light pollution, the biggest fraction of environmental photons comes from the sunlight reflected first by the moon and then by the earth [48].

$$N_{night}^{up} = A_E A_M R_M^2 a^2 \frac{\Omega_{fov}}{d_{EM}^2} B_f \Delta t H_{sun}. \quad (11)$$

Here  $A_M$  and  $R_M$  are the albedo and the radius of the Moon, while  $A_E$  is the albedo of the Earth and  $d_{EM}$  is the earth-moon distance.  $H_{sun}$  is the solar spectral irradiance in photons  $s^{-1}nm^{-1}m^{-2}$  at the wavelength of interest.  $\Omega_{fov}$  and  $a$  are angular field of view and radius of the receiving telescope.  $B_f$  is the width of the spectral filtering and  $\Delta t$  is the detection time-window.

For downlinks, the evaluation of the background photons is strongly site-dependent. The power received by the telescope can be expressed as follows

$$P_b = H_b \Omega_{fov} \pi a^2 B_f. \quad (12)$$

The parameter  $H_b$  is the total brightness of the sky background and it depends on the hour of the day and the weather conditions. From above equation, we derive the number of photons per time window

$$N^{down} = \frac{H_b}{h\nu} \Omega_{fov} \pi a^2 B_f \Delta t, \quad (13)$$

where  $h$  is the Planck constant and  $\nu$  is the frequency of the background photons (after filtering).

## 5 QBER

The QBER is a measure of the ratio of incorrect bit counts to the total number of received bit counts. It is used to quantify the probability of obtaining a false detection in comparison to the total probability of detection per pulse. The QBER is influenced by three main components: the signal component, the dark count component and the stray count component i.e. environmental photons.

### 5.1 QBER for BB84

In BB84 protocol, the QBER can be calculated as [48, 49]:

$$e_{84} = \frac{c p_{signal} + \frac{1}{2} (p_{dark} + p_{straycounts})}{p_{click}}. \quad (14)$$

Here,  $c$  corresponds to the error rate associated with depolarization in the encoding degree of freedom or imperfection of the preparation or detection stage leading to incorrect state discrimination. We chose a conservative value of  $c = 2\%$ ,  $p_{click}$  represents the overall anticipated probability that Bob will observe the detection of a photon during a specific pulse. Typically,  $p_{click}$  is determined by considering three distinct sources that can independently trigger a detection event. These sources encompass photons transmitted by Alice, background dark counts and straycounts.

$$p_{click} = p_{signal} + p_{dark} + p_{straycounts}. \quad (15)$$

Parameter	Value	Brief description
$t$	20 km	Atmospheric thickness
$H$	500 km	Minimum altitude (zenith)
$C_n^2$	$1.2 \times 10^{-16} m^{-2/3}$	Night time, clear weather
$C_n^2$	$1.64 \times 10^{-16} m^{-2/3}$	Day time, not windy
Sky brightness, $H_b$	$1.5 \times 10^{-6} W m^{-2} sr^{-1} nm^{-1}$	Night, clear sky
Sky brightness, $H_b$	$1.5 \times 10^{-3} W m^{-2} sr^{-1} nm^{-1}$	Day, clear sky
Field of view, $\Omega_{fov}$	$(100 \times 10^{-6})^2 sr$	Night-time downlink
Field of view, $\Omega_{fov}$	$(10 \times 10^{-6})^2 sr$	Day-time downlink
Field of view, $\Omega_{fov}$	$(30 \times 10^{-6})^2 sr$	Night-time uplink
Time Window $\Delta t$	0.5ns	Night and day time
Spectral filter width, $B_f$	1nm	Night-time downlink
Spectral filter width, $B_f$	0.2nm	Day-time downlink
Spectral filter width, $B_f$	1nm	Night-time uplink
$H_{sun}$	$4.610 \times 10^{18} phot s^{-1} nm^{-1} m^{-2}$	Solar spectral irradiance
$A_E$	0.300	Earth's albedo
$A_M$	0.136	Moon's albedo
$R_M$	$1.737 \times 10^6 m$	Moon's radius
$d_{EM}$	$3.600 \times 10^8 m$	Earth-moon distance

Table 1: Parameters related to the atmospheric weather conditions, stray photons and environmental light

The probability of Bob's detector firing due to a photon emitted by Alice's source is denoted as  $p_{signal}$  and is given by-

$$p_{signal} = 1 - \exp(-\eta_d \eta_T \mu), \quad (16)$$

where  $\eta_d$  is the detector efficiency,  $\eta_T$  is the total transmittance efficiency and  $\mu$  is the average number of photons per pulse. On the other hand,  $p_{dark}$  represents the probability of a dark count occurring in Bob's detector. Since each of Bob's detectors has a specific probability of dark counts per time slot in the absence of a real signal, the cumulative contribution of dark counts to the detection event is determined by the following relationship:

$$p_{dark} = 4d. \quad (17)$$

The presence of dark counts in the detection process is primarily determined by the characteristics of the detectors. Dark counts tend to become more significant when the probability of Bob's detector firing due to a photon from Alice's source,  $p_{signal}$  is small. Dark counts can arise from a source such as thermal fluctuations in the detector. In the equation mentioned above, the coefficient 4 is present because there are four detectors in the passive module, indicating that the dark count is four times larger than the parameter D. In addition, the number of dark counts occurring within the measurement time window can be expressed as four times larger than D. Furthermore, the dark count per measurement time window is given by a number of dark counts per measurement window:

$$d = Dt_w. \quad (18)$$

The equation mentioned above relates the dark counts per measurement time window to the dark count rate of the detectors, represented by  $D$ , and the duration of the measurement time window, denoted as  $t_w$ .  $p_{straycounts}$  is the probability of occurring straycounts which can be calculated using the expressions from Sec. 4. It is important to note that the Eq.(15) assumes the neglect of simultaneous occurrences of signal, dark count and straycounts events when all three  $p_{signal}$ ,  $p_{dark}$  and  $p_{straycounts}$  are small.

## 5.2 QBER for B92

The B92 protocol utilizes basis states to determine the code values. This results in 50% of cases using the same basis for coding and decoding, and 50% detecting differences in used bases. The number of usable bits equals 25% of the total received bits. The QBER parameters for the B92 protocol are as follows [49]:

$$e_{92} = \frac{c p_{\text{signal}} + \frac{1}{4} (p_{\text{dark}} + p_{\text{straycounts}})}{p_{\text{click}}}. \quad (19)$$

Here the parameters have the same definitions for  $p_{\text{signal}}$ ,  $p_{\text{dark}}$ ,  $p_{\text{straycounts}}$  and  $p_{\text{click}}$  as in the BB84 protocol.

## 5.3 QBER for BBM92

The QBER for BBM92 depends on various factors such as the properties of the quantum channel, the quality of the detectors used, and the presence of any eavesdroppers. In one beam splitter with transmission, we combine all losses to each receiver from the channel, detectors, and optics.

$$\alpha_L = \eta_{\text{det}} \cdot \eta_T. \quad (20)$$

The parameter  $\eta_{\text{det}}$  represents the detector efficiency of the system. The coincidence probability is divided into three components:  $p_{\text{true}}$ , which denotes the probability of a genuine coincidence between a pair of entangled photons,  $p_{\text{false}}$  which represents the probability of a false coincidence and  $p_{\text{straycounts}}$  which represents the probability of straycounts.

$$p_{\text{coin}} = p_{\text{true}} + p_{\text{false}} + p_{\text{straycounts}}. \quad (21)$$

We must choose a location for the source. Setting the source at a distance of  $L - x$  from Bob and  $x$  from Alice, we get

$$p_{\text{true}} = \alpha_x \alpha_{L-x} = \eta_{\text{det}} \alpha_L. \quad (22)$$

$$p_{\text{false}} = 4\alpha_x d + 4\alpha_{L-x} d + 16d^2. \quad (23)$$

Keeping only terms which are second order in  $\alpha_x$  and  $d$ , it can be observed that the probability of a true coincidence remains constant with respect to  $x$ , while the false coincidence rate changes. By performing a straightforward optimization, it can be determined that the false coincidence rate reaches its minimum value at a distance halfway between Alice and Bob. The value of this minimum false coincidence rate can be calculated using the given formula:

$$p_{\text{false}} = 8\alpha_{L/2} d + 16 d^2. \quad (24)$$

The QBER is given by

$$e_{M92} = \frac{c p_{\text{true}} + \frac{1}{2} (p_{\text{false}} + p_{\text{straycounts}})}{p_{\text{coin}}}. \quad (25)$$

## 5.4 QBER for E91

QBER for E91 is given by [11]

$$e_{91} = \frac{c p_{\text{true}} + \frac{1}{3} (p_{\text{false}} + p_{\text{straycounts}})}{p_{\text{coin}}}. \quad (26)$$

Here the parameters have the same definitions for  $p_{\text{true}}$ ,  $p_{\text{false}}$ ,  $p_{\text{straycounts}}$  and  $p_{\text{coin}}$  as in the BBM92 protocol. During the basis matching condition the unmatched basis is discarded to justify the protocol hence there is no contribution to QBER from this discarded key. A 1/3 chance of the basis matching with Bob exists since Bob and Alice selected three different bases. As a result, QBER will be impacted by a sifting factor of 1/3 .

## 6 Keyrate

Keyrate, in the context of QKD, refers to the rate at which a secure cryptographic key can be generated and shared between two communicating parties, typically referred to as Alice and Bob. It quantifies the speed or efficiency at which error-free key bits can be securely exchanged and determines the practicality and effectiveness of a QKD system. The key rate is measured in bits per second (bps) and is influenced by factors such as the quality of transmitted quantum states, detection efficiency, channel losses, and potential eavesdropping attempt. The keyrate serves as a benchmark for evaluating the effectiveness and practicality of protocols using QKD. In the calculation of keyrate, the QBER is considered, which includes all types of loss factors discussed earlier. The QBER, denoted by  $e$ , incorporates the effects of various loss factors, including geometrical loss, atmospheric losses like turbulence loss and scattering loss, and other factors that impact the security and performance of the QKD system are discussed above. By accounting for these losses in the QBER, the key rate provides a comprehensive assessment of the utility and efficiency of QKD protocols.

### 6.1 Keyrate for BB84

The secure key generation rate against photon number splitting (PNS) attack for the BB84 protocol is given by [50]:

$$R_{BB84} = \frac{1}{2} p_{click} \{ (1 - \tau' + f(e_{84})(e_{84} \log_2(e_{84}) + (1 - e_{84}) \log_2(1 - e_{84}))) \}. \quad (27)$$

and

$$\tau' = \tau \left( \frac{e_{84}}{\beta} \right), \quad (28)$$

where  $\beta$  security parameter defined as  $\beta = \left( \frac{p_{click} - p'}{p_{click}} \right)$  and

$$p' = 1 - \left( 1 + \mu + \frac{\mu^2}{2} + \frac{1}{2} \frac{\mu^3}{6} \right) \exp(-\mu). \quad (29)$$

$f(e_{84})$  is error correction factor [49],  $\tau$  is fraction of the key to be discarded during privacy amplification,  $\tau(e_{84}) = \log_2(1 + 4e_{84} - 4e_{84}^2)$  if  $e_{84} < 1/2$  and  $\tau(e_{84}) = 1$  if  $e_{84} > 1/2$ .

### 6.2 Keyrate for B92

The secure key generation rate of the B92 protocol against PNS attack can be formulated as [50]:

$$R_{B92} = \frac{1}{4} p_{click} \{ (1 - \tau' + f(e_{92})(e_{92} \log_2(e_{92}) + (1 - e_{92}) \log_2(1 - e_{92}))) \}. \quad (30)$$

In B92, only 25% of the bits transmitted will be detected by Bob, i.e., only 25% of the raw key bits should be kept. Hence  $\frac{1}{4}$  is the Sifting Factor. All the other expressions are defined in Sec. 6.1.

### 6.3 Keyrate for BBM92

The keyrate for BBM92 protocol against double blinding attack is given by [11]:

$$R_{BBM92} = \frac{p_{coin}}{2} \{ \tau(e_{M92}) + f(e_{M92})(e_{M92} \log_2(e_{M92}) + (1 - e_{M92}) \log_2(1 - e_{M92})) \}. \quad (31)$$

Due to the double-blinding attack discussed in Appendix C, Alice and Bob are unable to detect the presence of Eve, resulting in a complete elimination of information leakage. In other words, the measure of information leakage, denoted as  $\tau$  becomes zero in this scenario,  $f(e_{M92})$  is error correction factor,  $p_{coin}$  is the coincidence probability which has already been explained in Sec. 5.3.

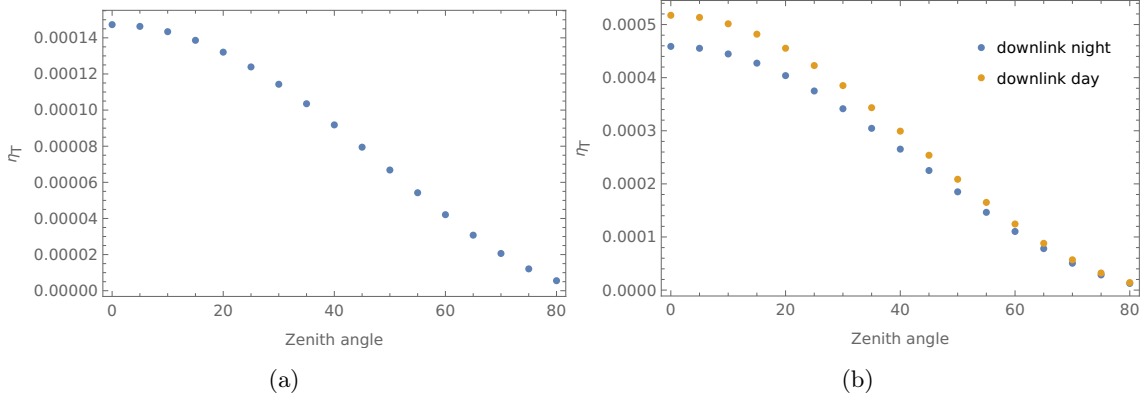


Figure 2: (a) Plot for transmittance with zenith angle for uplink night-time, (b) Plot for transmittance with zenith angle for downlink day and night-time.

## 6.4 Keyrate for E91

The keyrate for E91 protocol against double blinding attack is given by

$$R_{E91} = \frac{p_{coin}}{3} \{ \tau(e_{91}) + f(e_{91})(e_{91} \log_2(e_{91}) + (1 - e_{91}) \log_2(1 - e_{91})) \}. \quad (32)$$

Here  $\frac{1}{3}$  is sifting factor because we use three basis in E91. The parameters used in Eq.(32) have been described above.

## 7 Numerical Results and Discussion

We have analyzed the relationship between atmospheric transmittance and zenith angle, depicted in Fig. 2, considering uplink during night-time and both day-time and night-time for downlink. We have also done a comparison between the BB84 and B92 protocols and entangled based protocols BBM92 and E91 for both the uplink and downlink communication scenarios. Here we examine the relationship between zenith angle and two key metrics: the QBER and the keyrate. The simulated results, depicted in Figs. 3, 4, 5, and 6, showcase these dependencies for both the uplink and downlink scenarios.

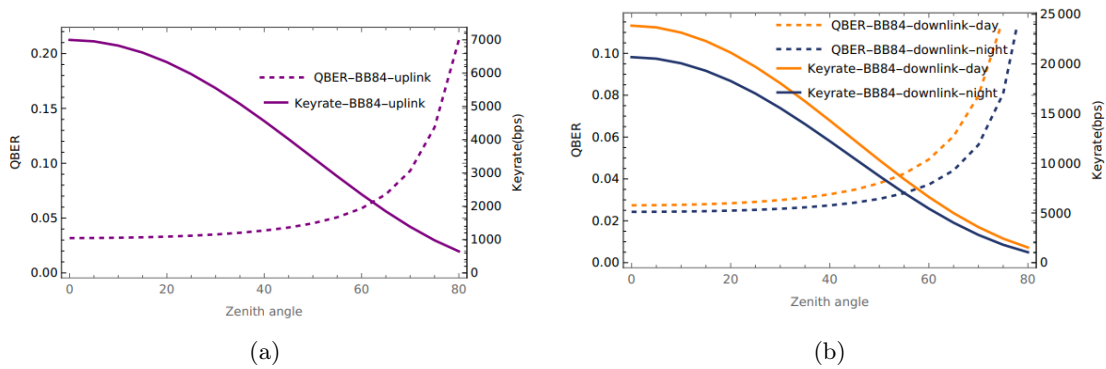


Figure 3: (a) Plot for QBER and keyrate for BB84 protocol with zenith angle for uplink night-time, (b) Plot for QBER and keyrate for BB84 protocol with zenith angle for downlink day and night-time.

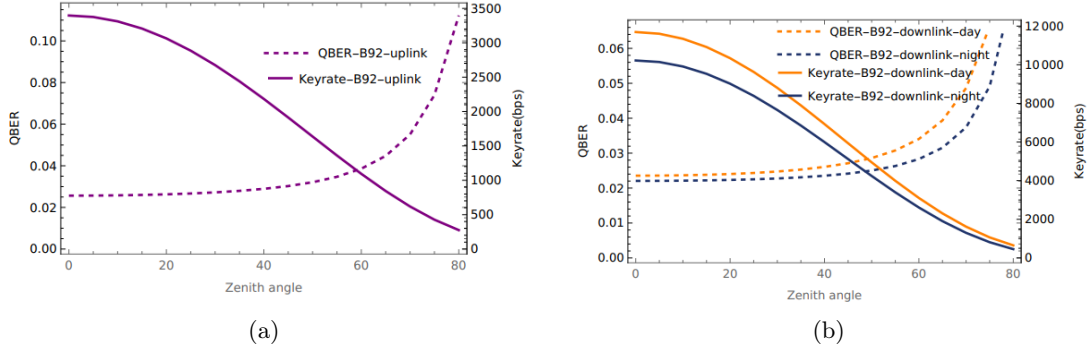


Figure 4: (a) Plot for QBER and keyrate for B92 protocol with zenith angle for uplink night-time, (b) Plot for QBER and keyrate for B92 protocol with zenith angle for downlink day and night-time.

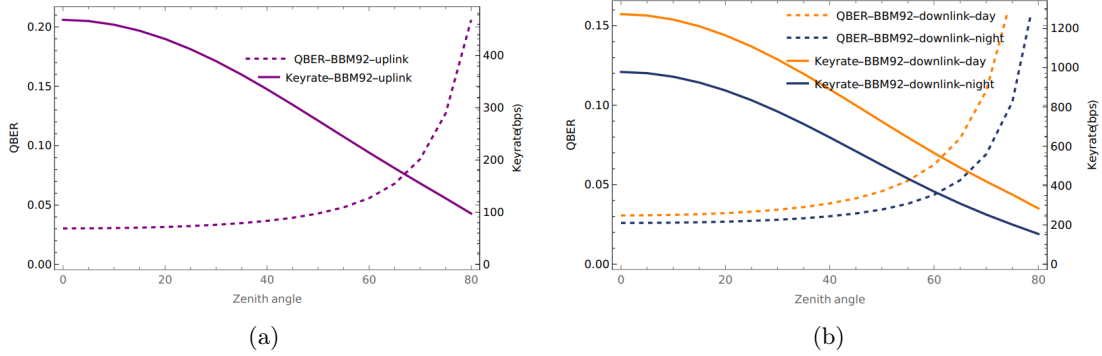


Figure 5: (a) Plot for QBER and keyrate for BBM92 protocol with zenith angle for uplink night-time, (b) Plot for QBER and keyrate for BBM92 protocol with zenith angle for downlink day and night-time.

We have done numerical simulations to investigate the QBER for laser links between a ground station and a satellite in low earth orbit. The simulations were performed at an operating wavelength of 800 nm, using a weak coherent source for the BB84 and B92 protocols, and an ideal entangled photon source for the BBM92 and E91 protocols. The dark count rate of the detector was set to  $4 \times 10^{-8}$ . The graph in *Fig.2* illustrates the decrease in atmospheric transmittance as the zenith angle increases for both the uplink and downlink scenarios. The comparison between day-time and night-time operation is particularly interesting. During the day, higher temperatures result in stronger wind and more active mixing between atmospheric layers, leading to more noticeable turbulence effects. However, clear days generally have lower moisture content in the lower atmosphere compared to nights, resulting in less beam spreading caused by scattering particles. On the other hand, at night, lower temperatures create a less turbulent atmosphere and also lead to the formation of haze and mist. In this scenario, the contribution of scattering caused by these particles can be more significant than the effects induced by turbulence. When comparing the uplink and downlink scenarios, the uplink experiences beam propagation through the turbulent atmosphere, leading to significant broadening, while the downlink only encounters turbulence during the final stage, resulting in less spreading. As a result, the attenuation in the uplink is more pronounced compared to the downlink due to these differing propagation conditions. Day-time uplink was not considered due to excessive background light. Comparing the uplink and downlink scenarios, the uplink consistently shows lower transmittance, primarily

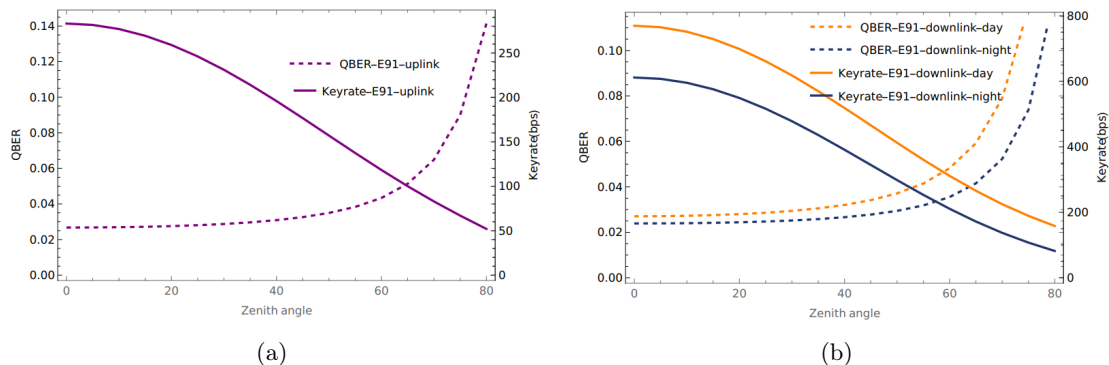


Figure 6: (a) Plot for QBER and keyrate for E91 protocol with zenith angle for uplink night-time, (b) Plot for QBER and keyrate for E91 protocol with zenith angle for downlink day and night-time.

due to increased turbulence as discussed above. Furthermore, during night-time downlink, transmittance is lower due to higher moisture content compared to day-time conditions. The plots shown in *Fig.3 – Fig.6* demonstrate that the QBER tends to increase and the keyrate tends to decrease as the zenith angle increases for both the uplink and downlink scenarios. Moreover, when comparing the uplink and downlink scenarios, it is evident that the QBER values are consistently higher and the keyrate is lower in the uplink for the aforementioned protocols. During day-time uplink, heightened background light causes an unacceptable increase in the QBER, prompting the exclusion of the related graph. Due to higher moisture content at night, both the QBER and keyrate are lower.

### Comparison performance of protocols:

**BB84 and B92:** Initially, at shorter atmospheric distances where the zenith angle is small for both BB84 and B92, their QBER are identical. However, the keyrate of BB84 is more as that of B92, indicating BB84 is better, as expected but as the atmospheric distance increases to around 70-80 degrees zenith angle, BB84 exhibits a higher QBER compared to B92. Therefore, in situations prioritizing heightened security over longer atmospheric distances, B92 outperforms BB84.

**BBM92 and E91:** At smaller zenith angles, there is a similarity observed in the QBER between the BBM92 and E91 protocols. Despite this similarity, the keyrate generated by BBM92 surpasses that of the E91 protocol, indicating a higher efficiency for BBM92. However, as the zenith angle increases significantly to approximately 70-80 degrees, a shift occurs: the QBER for BBM92 becomes notably higher than that of the E91 protocol. Consequently, this reversal in performance demonstrates that at higher zenith angles, E91 outperforms BBM92. The change in comparative efficiency between these protocols based on varying zenith angles showcases the dynamic nature of their performance characteristics, highlighting how their advantages and disadvantages manifest under different operational conditions.

## 8 Conclusion

The atmospheric transmittance relationship with zenith angle during uplink night-time and day-time/night-time downlink scenarios provides critical insights for laser communication between ground stations and low earth orbit satellites. A comparison was made between the BB84 and B92 protocols as well as BBM92 and E91 entangled based protocols for laser links between a ground station and a satellite in low earth orbit. The QBER calculation was done using various losses for all four protocols. The expressions for the quantum keyrate were given for the ideal single photon sources for BBM92 and E91 protocols. Similarly, the expressions for the quantum keyrate were given for the weak coherent sources for BB84 and B92 protocols.

On this basis, an evaluation of the quantum keyrate including various losses for the laser links between a ground station and a satellite for both uplink and downlink in the low earth orbit were performed. At lower zenith angles, the QBER across protocols like BB84 vs. B92 and BBM92 vs. E91 shows a striking similarity. However, there's a difference in the keyrate, such as in the comparison between BB84 and B92, where BB84 demonstrates a higher keyrate, suggesting its superior performance over B92. Conversely, when examining BB84 and B92 at higher zenith angles, BB84 exhibits a higher QBER than B92, causing B92 to outperform BB84 under these conditions. Similarly, in the comparison between BBM92 and E91, while BBM92 initially boasts a higher keyrate, at higher zenith angles, BBM92 shows a higher QBER, leading to E91 outperforming BBM92 in these scenarios. These findings highlight the dynamic nature of protocol efficiency under varying zenith angles, indicating the need for nuanced protocol selection based on operational conditions in ground-to-satellite and satellite-to-ground laser communication within low Earth orbit scenarios.

## Acknowledgements

The author would like to thank CSIR for the fellowship support. SB acknowledges support from Interdisciplinary Cyber Physical Systems (ICPS) programme of the Department of Science and Technology (DST), India, Grant No.:DST/ICPS/QuST/Theme-1/2019/6. SB also acknowledges the valuable contribution of the Defense Research and Development Organization (DRDO). The Author also wants to thanks Arindam Dutta for helpful discussions.

## Declarations

The authors declare no conflicts of interest related to this research.

## Data Availability Statement

Data sharing is not applicable to this article as no datasets were generated or analyzed during the current study.

## References

- [1] Anirban Pathak. *Elements of quantum computation and quantum communication*. CRC Press Boca Raton, 2013, Chapter-8.
- [2] Arockia Basil Raj, Vishal Sharma, and Subhashish Banerjee. Principle and applications of free space optical communication. *IET, UK*, 2019.
- [3] Dagmar Bruss, Gábor Erdélyi, Tim Meyer, Tobias Riege, and Jörg Rothe. Quantum cryptography: A survey. *ACM Computing Surveys (CSUR)*, 39(2):6–es, 2007.
- [4] S. Pirandola, U. L. Andersen, L. Banchi, M. Berta, D. Bunandar, R. Colbeck, D. Englund, T. Gehring, C. Lupo, C. Ottaviani, J. L. Pereira, M. Razavi, J. Shamsul Shaari, M. Tomamichel, V. C. Usenko, G. Vallone, P. Villoresi, and P. Wallden. Advances in quantum cryptography. *Advances in Optics and Photonics*, 12(4):1012, dec 2020.
- [5] Nicolas Gisin, Grégoire Ribordy, Wolfgang Tittel, and Hugo Zbinden. Quantum cryptography. *Rev. Mod. Phys.*, 74:145–195, 2002.
- [6] William K. Wootters and Wojciech H. Zurek. A single quantum cannot be cloned. *Nature*, 299:802–803, 1982.
- [7] N Srinatha, S Omkar, R Srikanth, Subhashish Banerjee, and Anirban Pathak. The quantum cryptographic switch. *Quantum Information Processing*, 13:59–70, 2014.
- [8] Charles H Bennett and Gilles Brassard. Quantum cryptography: Public key distribution and coin tossing. *arXiv preprint arXiv:2003.06557*, 2020.

- [9] Charles H. Bennett, François Bessette, Gilles Brassard, Louis Salvail, and John A. Smolin. Experimental quantum cryptography. *Journal of Cryptology*, 5:3–28, 1991.
- [10] W. T. Buttler, R. J. Hughes, P. G. Kwiat, S. K. Lamoreaux, G. G. Luther, G. L. Morgan, J. E. Nordholt, C. G. Peterson, and C. M. Simmons. Practical free-space quantum key distribution over 1 km. *Phys. Rev. Lett.*, 81:3283–3286, 1998.
- [11] Edo Waks, Assaf Zeevi, and Yoshihisa Yamamoto. Security of quantum key distribution with entangled photons against individual attacks. *Phys. Rev. A*, 65:052310, 2002.
- [12] Tobias Schmitt-Manderbach, Henning Weier, Martin Fürst, Rupert Ursin, Felix Tiefenbacher, Thomas Scheidl, Josep Perdignes, Zoran Sodnik, Christian Kurtsiefer, John G. Rarity, Anton Zeilinger, and Harald Weinfurter. Experimental demonstration of free-space decoy-state quantum key distribution over 144 km. *Phys. Rev. Lett.*, 98:010504, 2007.
- [13] Kishore Thapliyal, Anirban Pathak, and Subhashish Banerjee. Quantum cryptography over non-markovian channels. *Quantum Information Processing*, 16:1–21, 2017.
- [14] Vishal Sharma and Subhashish Banerjee. Analysis of atmospheric effects on satellite-based quantum communication: a comparative study. *Quantum Information Processing*, 18:1–24, 2019.
- [15] Theresa H Carbonneau and David Roger Wisely. Opportunities and challenges for optical wireless: the competitive advantage of free space telecommunications links in today’s crowded marketplace. *Wireless Technologies and Systems: Millimeter-Wave and Optical*, 3232:119–128, 1998.
- [16] Charles H Bennett, François Bessette, Gilles Brassard, and Louis Salvail. J.Smolin,“Experimental quantum cryptography”. *J. Cryptol*, 5(1):3–28, 1992.
- [17] Hugo Zbinden, Nicolas Gisin, Bruno Huttner, Antoine Muller, and Wolfgang Tittel. Practical aspects of quantum cryptographic key distribution. *Journal of Cryptology*, 13:207–220, 2000.
- [18] PCM Owens, JG Rarity, PR Tapster, D Knight, and PD Townsend. Photon counting with passively quenched germanium avalanche. *Applied Optics*, 33(30):6895–6901, 1994.
- [19] Kevin J Resch, M Lindenthal, B Blauensteiner, HR Böhm, A Fedrizzi, C Kurtsiefer, A Poppe, T Schmitt-Manderbach, M Taraba, R Ursin, et al. Distributing entanglement and single photons through an intra-city, free-space quantum channel. *Optics Express*, 13(1):202–209, 2005.
- [20] Dominic Mayers. Unconditional security in quantum cryptography. *Journal of the ACM (JACM)*, 48(3):351–406, 2001.
- [21] Andrew Shields and Zhiliang Yuan. Key to the quantum industry. *Physics World*, 20(3):24, 2007.
- [22] Mehrdad S Sharbaf. Quantum cryptography: An emerging technology in network security. In *2011 IEEE International Conference on Technologies for Homeland Security (HST)*, pages 13–19. IEEE, 2011.
- [23] WT Buttler, RJ Hughes, Paul G Kwiat, SK Lamoreaux, GG Luther, GL Morgan, JE Nordholt, CG Peterson, and CM Simmons. Practical free-space quantum key distribution over 1 km. *Physical Review Letters*, 81(15):3283, 1998.
- [24] Vishal Sharma, Chitra Shukla, Subhashish Banerjee, and Anirban Pathak. Controlled bidirectional remote state preparation in noisy environment: a generalized view. *Quantum Information Processing*, 14:3441–3464, 2015.
- [25] Jasmininder S Sidhu, Siddarth K Joshi, Mustafa Gündoğan, Thomas Brougham, David Lowndes, Luca Mazzarella, Markus Krutzik, Sonali Mohapatra, Daniele Dequal, Giuseppe Vallone, et al. Advances in space quantum communications. *IET Quantum Communication*, 2(4):182–217, 2021.
- [26] Sebastian Ecker, Bo Liu, Johannes Handsteiner, Matthias Fink, Dominik Rauch, Fabian Steinlechner, Thomas Scheidl, Anton Zeilinger, and Rupert Ursin. Strategies for achieving high key rates in satellite-based qkd. *npj Quantum Information*, 7(1):5, 2021.

- [27] Valentina Marulanda Acosta, Daniele Dequal, Matteo Schiavon, Aurélie Montmerle-Bonnefois, Caroline B Lim, Jean-Marc Conan, and Eleni Diamanti. Analysis of satellite-to-ground quantum key distribution with adaptive optics. *arXiv preprint arXiv:2111.06747*, 2021.
- [28] Christian Kurtsiefer, P Zarda, M Halder, Ph M Gorman, Paul R Tapster, JG Rarity, and Harald Weinfurter. Long-distance free-space quantum cryptography. In *Quantum Optics in Computing and Communications*, volume 4917, pages 25–31. SPIE, 2002.
- [29] Vishal Sharma. Effect of noise on practical quantum communication systems. *Defence Science Journal*, 66(2):186–192, 2016.
- [30] Robert Bedington, Juan Miguel Arrazola, and Alexander Ling. Progress in satellite quantum key distribution. *npj Quantum Information*, 3:1–30, 2017.
- [31] Vishal Sharma, U Shrikant, R Srikanth, and Subhashish Banerjee. Decoherence can help quantum cryptographic security. *Quantum Information Processing*, 17:1–16, 2018.
- [32] Vishal Sharma and Subhashish Banerjee. Analysis of quantum key distribution based satellite communication. In *2018 9th International Conference on Computing, Communication and Networking Technologies (ICCCNT)*, pages 1–5. IEEE, 2018.
- [33] Arindam Dutta and Anirban Pathak. Controlled secure direct quantum communication inspired scheme for quantum identity authentication. *Quantum Information Processing*, 22(13), 2022.
- [34] Arindam Dutta and Anirban Pathak. A short review on quantum identity authentication protocols: How would Bob know that he is talking with Alice? *Quantum Information Processing*, 21:369, 2022.
- [35] Richard J Hughes, Jane E Nordholt, Derek Derkacs, and Charles G Peterson. Practical free-space quantum key distribution over 10 km in daylight and at night. *New journal of physics*, 4(1):43, jul 2002.
- [36] Charles H. Bennett. Quantum cryptography using any two nonorthogonal states. *Phys. Rev. Lett.*, 68, 1992.
- [37] Artur K Ekert. Quantum cryptography based on bell’s theorem. *Physical Review Letters*, 67(6):661, 1991.
- [38] Charles H Bennett, Gilles Brassard, and N David Mermin. Quantum cryptography without bell’s theorem. *Physical Review Letters*, 68(5):557, 1992.
- [39] Abdulsalam G Alkholidi and Khalil S Altowij. Climate effects on performance of free space optical communication systems in yemen. *Frontiers of Optoelectronics*, 7:91–101, 2014.
- [40] Norhanis Aida M Nor, Md Rafiqul Islam, Wajdi Al-Khateeb, and AZ Suriza. Atmospheric effects on free space earth-to-satellite optical link in tropical climate. *International Journal of Computer Science, Engineering and Applications*, 3(1):17, 2013.
- [41] Nedasadat Hosseinidehaj. *Continuous-Variable Quantum Communication over Free-Space Lossy Channels*. PhD thesis, UNSW Sydney, 2017.
- [42] Harjeevan Singh and Nitin Mittal. Link budget analysis of free space optical communication link for atmospheric conditions of india. *Materials Today: Proceedings*, 48:1064–1069, 2022.
- [43] Sami M Sharif. Dust storms properties related to microwave signal propagation. *University of Khartoum Engineering Journal*, 1(1), 2011.
- [44] Zabih Ghassemlooy, Wasiu Popoola, and Sujun Rajbhandari. *Optical wireless communications: system and channel modelling with Matlab®*. CRC press, 2019.
- [45] Dirk Giggenbach and Hennes Henniger. Errata: Fading-loss assessment in atmospheric free-space optical communication links with on-off keying. *Optical Engineering*, 47(6):069801, 2008.
- [46] Larry C Andrews and Ronald L Phillips. *Laser beam propagation through random media*. 2005.
- [47] Hemani Kaushal, Georges Kaddoum, Virander Kumar Jain, and Subrat Kar. Experimental investigation of optimum beam size for fso uplink. *Optics Communications*, 400:106–114, 2017.

- [48] Carlo Liorni, Hermann Kampermann, and Dagmar Bruß. Satellite-based links for quantum key distribution: beam effects and weather dependence. *New Journal of Physics*, 21(9):093055, 2019.
- [49] Norbert Lütkenhaus. Security against individual attacks for realistic quantum key distribution. *Physical Review A*, 61(5):052304, 2000.
- [50] M.F. Abdul Khir, M.N. Mohd Zain, Iskandar Bahari, Suryadi, and S. Shaari. Implementation of two way quantum key distribution protocol with decoy state. *Optics Communications*, 285(5):842–845, 2012.
- [51] Samkelisiwe Purity Phehlukwayo, Marie Louise Umuhire, Yaseera Ismail, Stuti Joshi, and Francesco Petruccione. Influence of coincidence detection through free-space atmospheric turbulence using partial spatial coherence. *arXiv preprint arXiv:2006.12911*, 2020.
- [52] Hennes Henniger and Otakar Wilfert. An introduction to free-space optical communications. *Radio-engineering*, 19(2), 2010.
- [53] Arun Majumdar. Free-space laser communication performance in the atmospheric channel. *Journal of Optical and Fiber Communications Reports*, 2:345–396, 2005.
- [54] G. Adenier, Irina Basieva, Andrei Yu. Khrennikov, Masanori Ohya, and Noboru Watanabe. Double blinding-attack on entanglement-based quantum key distribution protocols. *Foundations of Probability and Physics*, 1424:9–16, 2011.

## Appendix A

### Turbulence Loss-Induced Scintillation loss for Uplink and Downlink

Scintillations are characterized by sudden and rapid changes in the phase and amplitude of a wave. These fluctuations occur due to the local and rapid variations in the refractive index of the medium through which the wave is traveling. When laser radiation propagates through a turbulent medium, it experiences both temporal and spatial fluctuations in irradiance, which are referred to as scintillation or atmospheric turbulence-induced irradiance fluctuations [51]. This phenomenon is a consequence of the random and irregular changes in the refractive index of the atmosphere that the laser beam encounters during propagation. The scintillation index is the most commonly used measure to quantify the magnitude of scintillation

$$\sigma_I^2 = \frac{\langle I^2 \rangle - \langle I \rangle^2}{\langle I \rangle^2} = \frac{\langle I^2 \rangle}{\langle I \rangle^2} - 1, \quad (33)$$

where  $I$  signifies the optical wave's irradiance and  $\langle \rangle$  stands for the ensemble average, which is equivalent to the long-time average if the process is assumed to be ergodic. The scintillation index in weak fluctuation theory is proportional to the Rytov variance given by:

$$\Sigma_1^2 = 1.23 C_n^2 k^{7/6} L^{11/6}, \quad (34)$$

where turbulence strength is measured by  $C_n^2$ ,  $k = \frac{2\pi}{\lambda}$ , is the optical wave number and  $L$  is the path length between the communication transmitter and receiver. The value of  $C_n^2$  is assumed to remain constant for horizontal paths up to a few kilometres, but for downlink (space-to-ground) and uplink (ground-to-space),  $h$  must be used. For vertical or slant path, the so-called Hufnagel-Valley model is generally regarded as representative of continental conditions [52].

### Hufnagel-Valley Model

We consider the generalized Hufnagel-Valley (HV) atmospheric-structure model.

$$C_n^2(h) = 0.00594 \left(\frac{v}{27}\right)^2 (10^{-5}h)^{10} \exp\left(-\frac{h}{1000}\right) + 2.7 \times 10^{-16} \exp\left(-\frac{h}{1500}\right) + A \exp\left(-\frac{h}{100}\right), \quad (35)$$

Here  $h$  is the altitude coordinate,  $v$  is a parameter related to high-altitude wind speed and  $A$  describes the relative strength of the turbulence near the ground level. Typical values are  $A = 1.7 \times 10^{-14} m^{-2/3}$  and  $v = 21 m s^{-1}$ . The value of  $C_n^2(h)$  inside the atmosphere in our model is estimated by the integral average of this function in  $[0, H]$ , rescaled by the fixed thickness  $t$ .

$$C_n^2 = \frac{1}{t} \int_0^H C_n^2(h) dh \quad (36)$$

The parameter  $v$  is kept fixed to the recommended value of  $21 m s^{-1}$ .  $A$  is chosen according to day and night,  $A_d = 2.75 \times 10^{-14}$  during the day and  $A_n = 1.10 \times 10^{-14}$  at night. Through Eq.(35), the first corresponds to  $C_n^2 = 1.64 \times 10^{-16} m^{-2/3}$  and the latter to  $C_n^2 = 1.12 \times 10^{-16} m^{-2/3}$ .

Scintillation loss of the transmission system (in dB) is given by [45]:

$$a_{sci} = [3.3 - 5.77(-\ln p_{thr})^{\frac{1}{2}}](\sigma_I^2(d_r))^{0.4}, \quad (37)$$

Here  $p_{thr}$  is the probability that the receiver power falls below the minimum received power.  $\sigma_I^2(d_r)$  is the aperture-averaged scintillation index. This is the factor which includes the concept of uplink and downlink. When it comes to the downlink of space-to-ground communications, the beam experiences distortion upon entering the Earth's atmosphere. The scintillation near the center of the received wave at ground level can be effectively represented and modeled as a plane wave.

For downlink, the aperture averaged scintillation index for plane wave is given by [53]:

$$\sigma_I^2(d_r) = \exp \left[ \frac{0.49 \Sigma_1^2}{\left(1 + 0.65d^2 + 1.11 \Sigma_1^{12/5}\right)^{7/6}} + \frac{0.51 \Sigma_1^2 (1 + 0.69 \Sigma_1^{12/5})^{-5/6}}{1 + 0.90d^2 + 0.62d^2 \Sigma_1^{12/5}} \right] - 1, \quad (38)$$

where  $\Sigma_1^2$  is the Rytov variance for plane wave and is given by above Eq.(34). Also,

$$d = \sqrt{\frac{K d_r^2}{4L}}, \quad (39)$$

where  $d_r$  is the receiver aperture size and  $K$  is the wave number. Further,  $L$  represents the distance between the transmitter and receiver in a communication system.

For an uplink, where the atmospheric turbulence begins just outside the transmitting aperture, we can assume a spherical wave and the expression for the apertured average scintillation index for spherical wave is given by [53]:

$$\sigma_I^2(d_r) = \exp \left[ \frac{0.49 \Sigma_2^2}{\left(1 + 0.18d^2 + 0.56 \Sigma_2^{12/5}\right)^{7/6}} + \frac{0.51 \Sigma_2^2 (1 + 0.69 \Sigma_2^{12/5})^{-5/6}}{1 + 0.90d^2 + 0.62d^2 \Sigma_2^{12/5}} \right] - 1, \quad (40)$$

where  $\Sigma_2^2$  is the Rytov variance for spherical wave and is given by:

$$\Sigma_2^2 = 0.4 \Sigma_1^2. \quad (41)$$

## Appendix B

### Turbulence-Induced Beam Wandering Effect

In the context of the uplink scenario for FSO from the ground to a satellite, the transmitter is located inside the Earth's atmosphere, while the receiver is positioned in the far field. In this configuration, the size of the transmitter beam is typically smaller than the outer scale of turbulence, known as  $L_0$ . Consequently, the instantaneous point of maximum irradiance, often referred to as the "hot spot," will be displaced from its

original on-axis position. As a result, this displacement of the "hot spot" due to the beam size being smaller than the eddies' size can cause a pointing error, leading to the misalignment of the beam and missing the intended target. When the eddies' size is smaller than the beam size, only a small fraction of the beam will undergo diffraction and scattering independently.

In ground-to-satellite FSO communication, the laser beam encounters random inhomogeneities in the atmosphere caused by fluctuations in the refractive index. These fluctuations are quantified by the refractive index structure parameter, described above as  $C_n^2(h)$ , which characterizes the strength of turbulence in the atmosphere at different heights above the ground. Obtaining accurate measurements of  $C_n^2(h)$  is crucial and can be achieved by measuring parameters such as temperature ( $T$ ), pressure ( $P$ ), wind speed ( $v$ ), and spatial fluctuations in temperature ( $\Delta T$ ) along the propagation path [47]:

$$C_n^2 = \left[ 79 \times 10^{-6} \frac{P}{T^2} \right] C_T^2, \quad (42)$$

here  $C_T^2$  is the temperature structure parameter which is determined by taking the measurements of mean square temperature between two points separated by certain distance along the propagation path (in  $deg^2/m^{-2/3}$ ) and is expressed as:

$$C_T^2 = \langle \Delta T^2 \rangle r^{-1/3}, \quad (43)$$

where  $\Delta T = T_1 - T_2$  ( $T_1$  and  $T_2$  are the temperatures of two arbitrary points separated by a distance  $r$ ) and the angle bracket  $\langle \rangle$  denotes an ensemble average. The Profile model of the refractive index structure parameter ( $C_n^2(h)$ ) describes how it varies with altitude ( $h$ ). Turbulence in the atmosphere gives rise to the formation of eddies with different refractive indices and sizes. In the FSO uplink scenario, when the beam size is smaller than the outer scale of turbulence ( $L_0$ ), the entire beam undergoes random deflection from its original path. This phenomenon, known as beam wander, results in a significant change in the direction of the beam. The statistical characterization of the beam wander effect is represented by the variance of beam wander displacement ( $\langle r_c^2 \rangle$ ) and can be expressed as: [47]

$$\langle r_c^2 \rangle = 0.54(H - h_0)^2 \sec^2(\theta) \left( \frac{\lambda}{2W_0} \right)^2 \left( \frac{2W_0}{r_0} \right)^{5/3}, \quad (44)$$

where  $\theta$  is the zenith angle,  $\lambda$  is the operating wavelength,  $W_0$  is the transmitter beam radius,  $H$  and  $h_0$  are the altitude of satellite and transmitter respectively. For ground based transmitter,  $h_0 = 0$  and satellite altitude  $H = h_0 + L(\cos(\theta))$  where  $L$  is propagation length. The other parameter  $r_0$  is the atmospheric coherence length (or Fried parameter) defined by:

$$r_0 = \left[ 0.423K^2 \sec(\theta) \int_{h_0}^H C_n^2(h) dh \right]^{-3/5}, \quad (45)$$

where  $K$  is the optical wave number.

The beam wander effect will lead to effective pointing error of the beam  $\sigma_{Pe}$  given as[47]

$$\sigma_{Pe}^2 = \langle r_c^2 \rangle \left[ 1 - \left( \frac{C_r^2 W_0^2 / r_0^2}{1 + C_r^2 W_0^2 / r_0^2} \right)^{1/6} \right]. \quad (46)$$

In the above equation, the parameter  $C_r$  is a scaling constant typically in the range from 1 to  $2\pi$ . The pointing error induced by beam wander contributes to an increase in the scintillation index, which differs from the prediction of conventional Rytov theory. In the first-order Rytov theory, the scintillation index, denoted as  $\sigma_I^2$ , is expressed as the sum of longitudinal  $\sigma_{I,l}^2$  and radial  $\sigma_{I,r}^2(r, l)$  components. However, when accounting for the beam wander effect in FSO uplink scenarios, the increase in  $\sigma_{I,l}^2(L)$  should be considered. This is because the effect of beam wander can cause slight flattening of the beam and an increase in the long-term beam profile near the bore-sight.

The Scintillation produced by beam wander effect is expressed as[47]:

$$\sigma_{I,l}^2(L) = 5.95(H - h_0)^2 \sec^2(\theta) \left( \frac{2W_0}{r_0} \right)^{5/3} \left( \frac{\alpha_{Pe}}{W} \right)^2. \quad (47)$$

In the above equation,  $\alpha_{Pe} = \sigma_{Pe}/L$  is the angular pointing error due to beam wander effect.

## Appendix C

### Blinding Attacks (Single and Double Blinding Attacks)

In the context of the BBM92 protocol, the existing blinding attack are of the intercept and resend type. In this type of attack, a malicious entity, often referred to as Eve, intercepts the signal that was originally intended for Bob. Eve then proceeds to perform measurements using random bases in order to obtain the raw key, just as Bob would have done in the intended communication process. To conceal her presence, Eve forwards a signal to Bob whenever she successfully obtains a measurement result. This signal ensures that Bob receives an identical outcome, while in the case of diagonal alignment, no detection occurs at all. In practical implementation using QKD devices [54], Eve employs techniques to blind Bob's detectors to single-photon detection. She achieves this by manipulating the detectors to shift from Geiger mode to linear mode, where a detector only registers a click if the incoming signal intensity exceeds a preset discriminator threshold, denoted as  $I_{th}$ . After each detection, Eve sends a bright pulse with linear polarization aligned to her own measurement result. When Eve and Bob randomly select identical measurement bases, the pulse deterministically generates a click in one of Bob's detectors. This ensures that Bob's measurement outcomes match those of Eve because the pulse is either fully reflected or transmitted at Bob's polarizing beamsplitter. However, to prevent double counting and incorrect results when Eve and Bob randomly select bases that are diagonal to each other, Eve adjusts the intensity of the pulses to be lower than twice the threshold intensity of the detectors. Consequently, the pulse is split in half at Bob's polarizing beamsplitter, resulting in an output that is insufficient to surpass the threshold and produce a click in either of Bob's detectors. The objective of the attack is for Eve to obtain an exact replica of Bob's key at the conclusion of the raw key distribution process. If Alice and Bob are sufficiently satisfied with the measured QBER on a subset of the key, Eve can eavesdrop on the error correction protocol that Alice and Bob employ. By performing the same operations as Bob during the error correction phase, Eve can successfully acquire an exact copy of the sifted key in the end. One limitation of single-blinding attacks is that, on average, Bob's resulting key size is reduced by half compared to what he would have obtained without the attack. This reduction occurs because approximately half of the time, the randomly chosen measurement bases of Eve and Bob turn out to be diagonally opposite to each other. Consequently, Bob's detectors do not register any clicks in such cases. Therefore, the efficiency of this attack, by design, is fundamentally limited to 50% on Bob's side.

Here the proposed double-blinding attack involves a similar implementation to the single-blinding attack, but with the key difference that Eve blinds all detectors on both sides instead of just Bob's detectors. Due to the double-blinding attack, Alice and Bob are unable to detect the presence of Eve, resulting in a complete elimination of information leakage. In other words, the measure of information leakage, denoted as  $\tau$  becomes zero in this scenario.